Proceedings of the 17th International Heat Transfer Conference, IHTC-17
14 – 18 August 2023, Cape Town, South Africa

IHTC-17 | ID: 246

FLOW BOILING IN A MICROGAP AND MICRO MULTI-CHANNEL HEAT EXCHANGER

Ali H. Al-Zaidi[1], Mohamed M. Mahmoud[2], Atanas Ivanov[3], Tassos G. Karayiannis[3*]

[1]University of Misan, Al-Amarah, 62001, Iraq
[2]Faculty of Engineering, Zagazig University, Zagazig, 44519, Egypt
[3]Department of Mechanical and Aerospace Engineering, Brunel University London, Uxbridge, UB8 3PH, UK

ABSTRACT

Two-phase flow in micro scale heat exchangers is considered a promising cooling technique for electronic and other high heat flux devices. Different operating conditions and heat exchanger geometries can lead to different flow patterns, pressure drop and heat transfer characteristics. The performance of two different designs was examined in this study, namely: a microgap and a micro multi-channel configuration. Both heat sinks were manufactured from oxygen-free copper using a high precision micro-milling machine. The microgap was 1 mm high, 20 mm wide and 25 mm long, i.e. had a base area of 20 × 25 mm^2, with the fluid entering and exiting vertically in the inlet and outlet plenum. The micro multi-channel heat sink had the same base area, with 40 channels, 0.7 mm high, 0.35 mm wide separated by a wall 0.15 mm thick, with the fluid entering and exiting vertically in the plena. The base heat flux ranged from 34 to 440 kW/m^2, while the mass flux varied from 100 to 200 kg/m^2 s. The inlet sub-cooling was kept low, at 5 K for both heat sinks. The experiments were performed at atmospheric system pressure. The working fluid used was HFE-7100, a dielectric and eco-friendly refrigerant. Flow visualization was carried out using a high-speed, high-resolution camera. The flow patterns, heat transfer coefficient and pressure drop for the two geometries were obtained and compared. The performance index, i.e. the ratio of the heat transfer rate to the total pressure drop, was also calculated and compared for the two examined geometries.

KEY WORDS: Two-phase flow, micro scale, multi-channels, microgap, performance index.

1. INTRODUCTION

Effective cooling systems are necessary to meet the increasing thermal loads that need to be dissipated from a small area in electronic equipment and other high heat flux devices [1]. These systems should achieve high heat transfer rates, low and uniform substrate temperature, low power consumption, high thermal performance and use eco-friendly and dielectric refrigerants. Two-phase flow boiling in micro scale pumped systems can meet most of the necessary design requirements for an effective cooling system. However, the fundamentals of two-phase flow in micro scale heat sinks are not fully understood and more numerical and experimental investigations are needed. The shape of heat sink or channel geometry is one of the critical issues that can affect the thermal performance of the cooling system. Therefore, different geometries were proposed and examined in the literature. For example, rectangular micro multi-channels were tested by [2]-[3], micro pins having different shapes were examined by [4]-[5] and wavy channels were studied by [6]-[7]. The microgap heat sink is considered a simple design and of low cost compared to other geometries, see [8]-[9] for flow boiling heat transfer and pressure drop results. The present experimental study aimed to investigate and compare the thermal performance of two different heat sink geometries, namely a microgap and a micro multi-channel heat sink using HFE-7100.

*Corresponding Author: tassos.karayiannis@brunel.ac.uk

2. EXPERIMENTAL FACILITY AND PROCEDURE

The experimental facility consisted of a liquid reservoir, sub-cooler, micro-gear pump, Coriolis flow meters, pre-heater, test section, visualization system and chiller system, see Fig. 1 and reference [10] for further details. The visualization system included a Phantom high-speed, high-resolution camera having a frame rate of 1800 fps at a resolution of 1280 × 1024 pixel. The camera was mounted on a microscope with LED lighting system. A set of measuring instruments, such as pressure transducers, thermocouples and flow meters, were carefully calibrated and connected to the Data Acquisition System. The data were collected at a frequency of 1 kHz. All the measured data were recorded and saved to a computer using LabVIEW software for two minutes. This was carried out when the steady state was reached, i.e. the variation in the measured signals such as temperature, mass flow rate and pressure was within 5%, during at least 3 minutes.

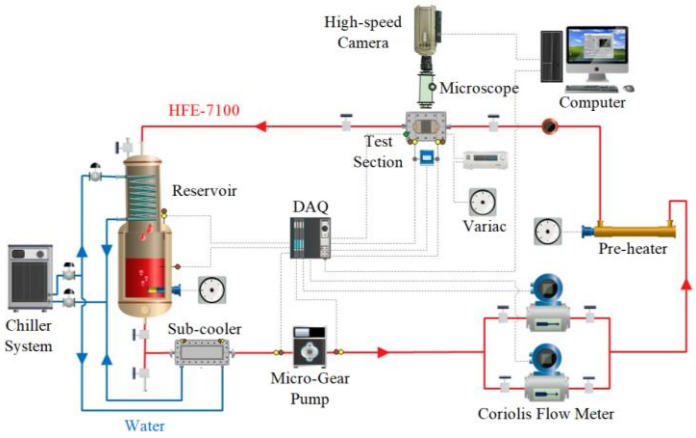

Fig. 1 Schematic diagram of the experimental facility [10].

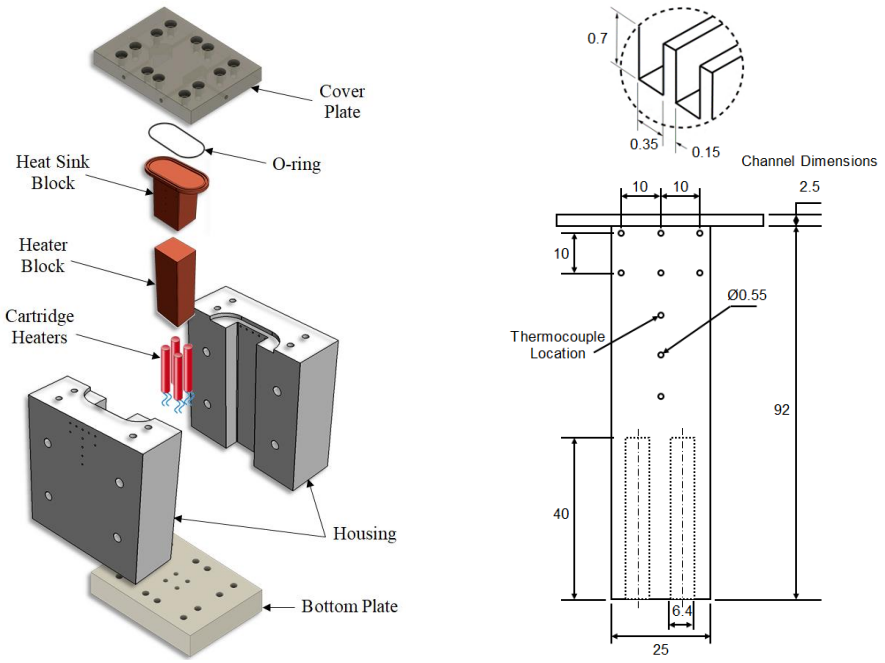

(a) (b)

Fig. 2 Test section: (a) Exploded drawing (b). Dimensions in mm. Note: five thermocouples in the microgap - two at 2.5 mm from each end and the other three equidistant 5 mm apart [10].

Fig. 2 shows the construction of the test section that consisted of the bottom plate, housing, cartridge heaters, the oxygen-free copper heat sink and the cover plate. Both the bottom plate and the housing were made of PTFE to minimize the heat loss, while the cover plate was made of a transparent polycarbonate sheet to allow flow visualization. This cover plate also housed the inlet/outlet fluid tubes, inlet/outlet fluid thermocouples and inlet/outlet pressure ports. Four vertical cartridge heaters were inserted inside the heater block to supply the required heating power. The heat sink block was then attached on the heater block with thermal paste (RS 503-357) between them. An O-ring was placed between the heat sink and the cover plate to prevent any leakage during the experiments. A set of thermocouples were inserted into the heat sink block to measure the temperatures, with the readings used to calculate the supplied heat flux and the wall temperature. Inlet/outlet pressure transducers and one differential pressure transducer were also connected to the test section to measure the inlet/outlet fluid pressure and the total pressure drop inside the heat sink. A high-precision milling machine was used to fabricate a microgap heat sink having 1 mm height, 20 mm width and 25 mm length. The micro multi-channel heat sink was manufactured having forty channels and 0.7 mm height, 0.35 mm width separated by a fin thickness of 0.15 mm. These two heat sinks had the same total base area of 500 mm^2 with the fluid entering and exiting vertically. The surface roughness measurements of the microgap and multi-channel heat exchanger were carried out using a Mitutoyo Surftest Perthometer and had an average value of 0.12 and 0.1 μm, respectively. The present experimental study was carried out at an inlet pressure of 1 bar and inlet fluid temperature 55 °C (5 K sub-cooling). The mass flow rate was changed from 0.97×10^{-3} to 4×10^{-3} kg/s to achieve a mass flux (based on the microgap and channel free-flow cross-sectional area) of 100−200 kg/m^2 s. The base heat flux was increased gradually until an exit vapour quality of one or the critical heat flux was reached. The range covered was from 34 to 440 kW/m^2. The critical heat flux was identified during the experiments, when the wall temperatures along the heat sink increased suddenly with time.

3. DATA REDUCTION AND UNCERTAINTY

Single-phase experiments were first conducted to validate the experimental system. Both the experimental fanning friction factor and the average Nusselt number were calculated using Eq. (1) and (2), respectively.

$$f_{exp} = \frac{\Delta P_{ch} D_h}{2 L_{ch} v_l G_{ch}^2} \tag{1}$$

$$\overline{Nu}_{exp} = \frac{\overline{h}_{exp} D_h}{k_l} \tag{2}$$

The flow Reynolds number was calculated using Eq. (3) below:

$$Re = \frac{G_{ch} D_h}{\mu_l} \tag{3}$$

The channel pressure drop was found from Eq. (4).

$$\Delta P_{ch} = \Delta P_{meas} - (\Delta P_{sc} + \Delta P_{se}) \tag{4}$$

where ΔP_{meas}, ΔP_{sc} and ΔP_{se} are the measured total pressure drop in the heat sink (from the differential pressure transducer), the sudden contraction pressure drop at the channel inlet and the sudden expansion pressure drop at the channel outlet, respectively. For the multi-channels, both pressure drop components of sudden contraction and sudden expansion were calculated using equations reported in ref. [11], while these two components were excluded from the microgap calculations. Eq. (5) was used to find the local heat transfer coefficient at each location and along the heated length.

$$h_{(z)} = \frac{q_b^{"} A_b}{A_{ht}(T_{wi(z)} - T_{f(z)})} \tag{5}$$

The average heat transfer coefficient $\overline{h}_{exp}$ was calculated by integrating the local heat transfer coefficient along the heat sink. The vertical temperature gradient obtained from the five thermocouples embedded in the heater block in the vertical direction was used to calculate the base heat flux, see Eq. (6). The local internal surface temperature can be calculated from Eq. (7) at 5 and 3 different locations along the flow direction for the microgap and the multi-channels, respectively.

$$q_b^{"} = k_{cu} \frac{dT}{dy} \tag{6}$$

$$T_{wi(z)} = T_{th(z)} - \frac{q_b^{"} * Y}{k_{cu}} \tag{7}$$

The local fluid temperature was calculated from the energy balance at each location. This temperature was replaced by the local saturation temperature for the two-phase flow region. The local saturation temperature

was found from the corresponding local pressure by assuming linear pressure drop between the end of the single-phase region and the exit. An energy balance was used to calculate the length or extend of the single-phase flow from the entry point to the channels, see [2] and [10] for further details. The single-phase pressure drop ΔP_{sp} to that point was calculated using Eq. (1) with the known f_{exp} and with L_{sp} replacing L_{ch}. The two-phase pressure drop ΔP_{tp} was then calculated from Eq. (8).

$$\Delta P_{tp} = \Delta P_{ch} - \Delta P_{sp} \tag{8}$$

The performance index PI was found as follows:

$$PI = \frac{Q_{eff}}{\Delta P_{meas}} \tag{9}$$

The effective heat transfer rate Q_{eff} was calculated by multiplying the base heat flux by the base area. The experimental uncertainties were calculated using a method described in [12], and the maximum uncertainty in the friction factor, average Nusselt number, wall heat flux and average heat transfer coefficient were found to be 13%, 14.5%, 15% and 14%, respectively.

4. RESULTS AND DISCUSSION

4.1 Single-phase validation

Both adiabatic and diabatic single-phase experiments were carried out to validate the experimental rig. The fanning friction factor and the average Nusselt number were calculated and plotted versus Reynolds number, as shown in Fig. 3. It can be seen from this figure that, the experiments were within the laminar flow region, i.e. Reynolds number < 2300. A very good agreement between the experimental results and the existing correlations was found, such as the one proposed by Shah and London [13] (for calculating the Fanning friction) and Peng and Peterson [14] (for calculating the average Nusselt number). In addition to the single-phase validation, a degassing process was conducted before the boiling experiments to ensure a pure refrigerant without any trapped air.

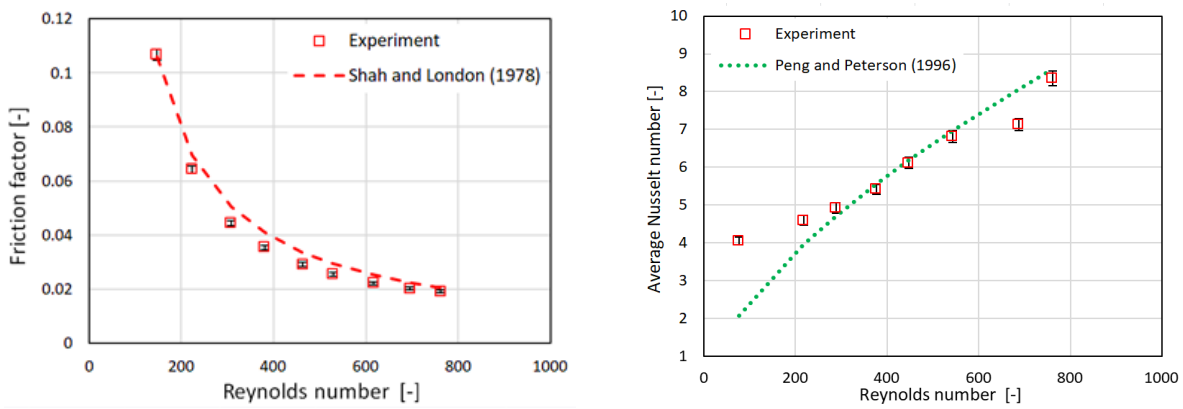

Fig. 3 Single-phase validation using micro multi-channels.

4.2 Experimental flow boiling patterns

***Multi-channels*:** Flow visualization was carried out at different locations along the heat sink (inlet, middle and outlet). Generally, four flow patterns were visualised inside the micro multi-channels as shown in Fig. 4, i.e. bubbly, slug, churn and annular flow. Nucleating bubbles were first activated at the channel corners, with more on the entire surface with increasing heat flux. When these bubbles became confined, the flow changed to long vapour slugs. Churn flow, as a mixture of liquid and vapour, and annular flow, as a vapour core surrounded by liquid film, were also seen. Results at a lower heat flux are also seen in Fig. 6 of [10] where bubbly and slug flow as well as churn and annular flows are shown more prominently.

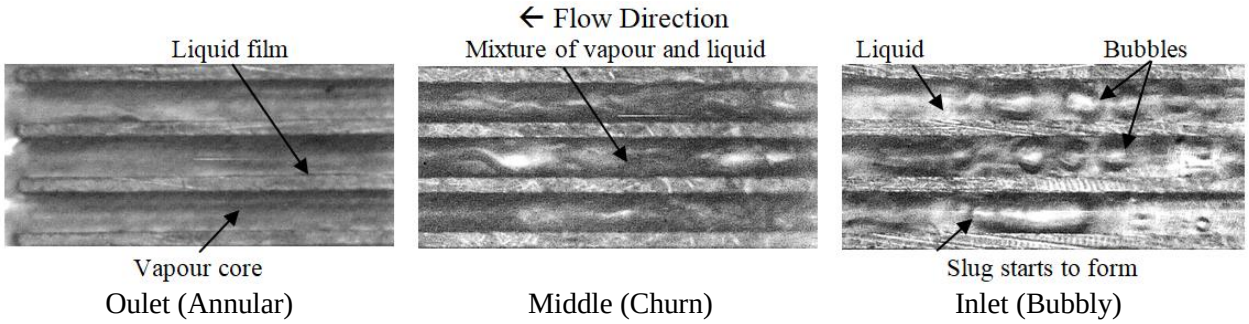

Fig. 4 Flow patterns in the multi-channels at wall heat flux of 126 kW/m^2 and mass flux of 200 kg/m^{2}s.

***Microgap*:** The prevailing flow patterns were found to be completely different from the multi-channel heat exchanger, see Fig. 5. Nucleating bubbles first appeared at the edges of the heat sink (from both sides). New nucleating bubbles were also activated on the bottom surface with increasing heat flux. It is worth mentioning that these bubbles were originally located at the surface cutting marks. The bubble coalescence rate at the edges, where most of the bubble generation first starts, was very high and led to vapour layers. These layers were captured to move from the edges to the central flow stream in a zigzag manner, i.e. the flow moved forward while fluctuating from left to right. Dryout spots underneath these layers were visualized when these vapour layers became large and covered the surface. The transition flow included a mixture of liquid, small bubbles and large flattened (i.e. squeezed) vapour bubbles. This was the result of bubble coalescence, with the larger bubbles squeezed between the cover plate and the bottom surface. Dryout spots were also seen underneath these bubbles. It is worth mentioning that slug flow similar to that observed in the microchannels was not found in the microgap. This could be due to the fact that the vapour bubbles were not confined by the channel sidewalls. The squeezed bubbles mentioned above, developed to a large vapour layer that filled the space between the cover plate and the surface bottom, with dryout spots and liquid straps visualized underneath this layer. When the heat flux increased to 167 kW/m^2, entire large dry areas were seen. Accordingly, the size of the liquid straps reduced due to liquid evaporation and turned to liquid droplets on the surface bottom. At this stage, a sudden jump in the wall temperature was recorded leading to critical heat flux. Annular flow, as a vapour core surrounding by a liquid film, was not clearly observed during the present study. Therefore, this term was not used to describe the observed flow regimes. It is worth mentioning that, annular flow in microgap heat sinks was observed and reported in the literature, see [15], [9], [16] and [17]. However, de-ionised water as a working fluid was tested in these studies, which could result in different features of flow patterns compared to HFE-7100.

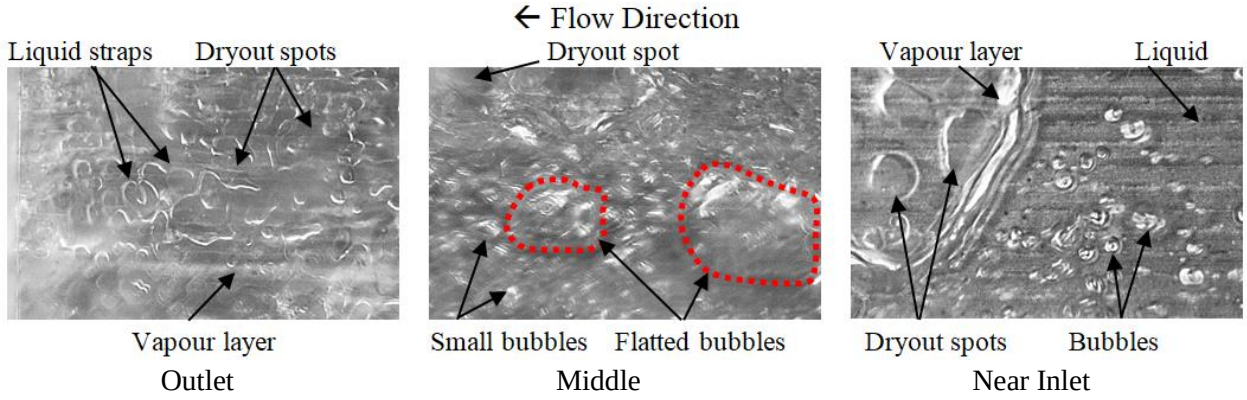

Fig. 5 Flow patterns in the microgap at wall heat flux of 130 kW/m^2 and mass flux of 200 kg/m^2 s.

4.3 Two-phase heat transfer

The average and local heat transfer coefficient versus wall heat flux for the mass flux of 200 kg/m^{2}s is plotted in Fig. 6. The figure shows that, for both heat sinks, the average two-phase heat transfer coefficient increased with increasing wall heat flux due to the large bubble generation and liquid film evaporation. This was also found for other mass fluxes studied. However, for the microgap heat sink, the average heat transfer coefficient decreased after a wall heat flux of 225 kW/m^2, indicating the approach to the critical heat flux condition. A sudden jump in the wall temperature can be seen in this region, i.e. 4 K temperature difference between the last three points in the graph. The prevalent flow pattern at this stage was a vapour layer with many and large dry areas on the surface. These hot spots led to an increase in the surface temperature resulting in lower heat transfer coefficient. As also seen in the figure, for a given wall heat flux, the multi-channels resulted in higher local and average heat transfer coefficient compared to the microgap. This could be the result of the different flow patterns and hence heat transfer mechanisms that prevail in the two heat sinks. Nucleating bubbles were observed in both heat sinks, however other features were different. In the multi-channel heat sink bubbles were first generated at the channel corners and with the entire surface becoming active with increasing heat flux, Al-Zaidi et al. [18]. In other words, the existence of the channels and thus the corners resulted in a larger number of bubbles for a given heat flux. The heat transfer coefficient in flow boiling is higher in the nucleate boiling dominant region. Furthermore, flow visualization showed that dryout spots and vapour layers were also generated during these nucleating bubbles in the microgap, as discussed in Section 4.2, reducing the heat transfer rates. With further increase in heat flux or at the outlet, large dryout spots and liquid straps on the gap surface were clearly captured by the high-speed camera. These features were not seen in the multi-channel heat sink. The increase in the average heat transfer coefficient was found to be 21% (average value for the range 50 to135 kW/m^2, i.e. common range of wall heat flux range of figure 6).

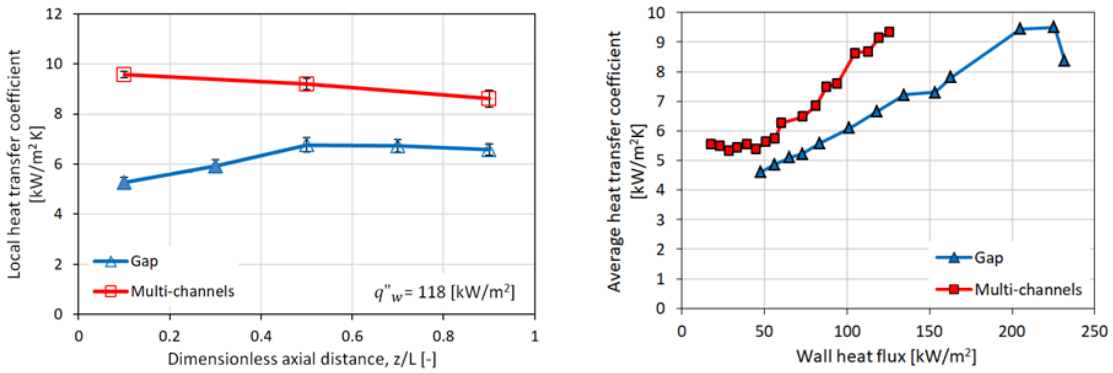

Fig. 6 Local and average heat transfer coefficient at mass flux of 200 kg/m^{2}s. Filled and empty markers refer to local heat transfer coefficients measured in the subcooled and saturated boiling region, respectively.

4.4 Two-phase pressure drop

The two-phase pressure drop for the microgap and multi-channels was calculated and plotted in Fig. 7 at a mass flux of 200 kg/m^{2}s. As seen in the figure, the two-phase pressure drop was found to increase with increasing wall heat flux for both heat sinks. High flow resistance due to the large bubble generation and coalescence rate with increasing heat flux could result in an increase in the pressure drop components. It is worth mentioning that, for the microgap heat sink, the two-phase pressure drop is small and tends to a constant value as the heat flux increases. This figure also shows that the two-phase pressure drop in the multi-channels was much larger than that in the microgap. The mean absolute difference between the two heat sinks was 550% for the heat flux range of 50−135 kW/m^2. The confinement effect by the rectangular multi-channels could lead

to high flow resistance, i.e. flow is confined by channel sidewalls, and hence large pressure drop in the multi-channel heat sink. The pressure fluctuations in the microchannels were also higher, due possibly to flow reversal, see [10].

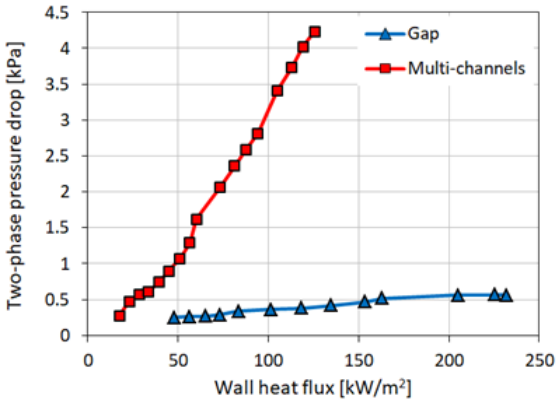

Fig. 7 Two-phase pressure drop at mass flux of 200 kg/m^2 s.

4.5 Thermal performance

The thermal performance of these two heat sinks can also be assessed by presenting the boiling curve and the performance index, see Fig. 8. The boiling curve was presented by plotting and comparing the base heat flux versus wall superheat (at the middle of the heat sink). The saturation temperature (T_{sat} = 61 °C) was the same in both test sections, i.e. same system pressure. Fig. 8(a) depicts that the base heat flux increased with wall superheat for both heat sinks. The base heat flux in the multi-channels was found to be higher for a given wall superheat. The large total heat transfer area with area ratio of 3.2 due to the microchannel fins contributes to this higher value. A base heat flux of 440 kW/m^2 was reached using this heat sink at a mass flux of 200 kg/m^{2}s, without an indication of reaching critical heat flux conditions. At the same mass flux of 200 kg/m^{2}s, the maximum base heat flux was found to be only nearly 250 kW/m^2 in the microgap, i.e. critical heat flux was reached in this heat sink at this value. This figure also shows that, the maximum wall temperature reached was 74 °C and 88 °C in the multi-channels and microgap, respectively. It is clear therefore that the multi-channel heat sink provides both lower temperatures for a given load and higher possible heat flux due to both the area enhancement and the different prevailing flow patterns - nucleate boiling and film evaporation without large dryout areas. It is worth mentioning that, Kandlikar et al. [19] also found that the heat transfer performance of multi-channels was much better than that in the plain surface (gap). Their results showed that, larger heat flux was achieved in the multi-channel heat exchanger at a given wall superheat. In addition, critical heat flux was reached at lower values in the plain surface test section. Kandlikar et al. [19] noted that this different behaviour was due to the dryout areas under nucleating bubbles found in the plain surface and different heat transfer area; in agreement with the above observations. The performance index of both heat sinks was found to be completely different, see Fig. 8(b). The trend of the multi-channels showed a reduction in this index with increasing base heat flux. This was due to the large increase in the pressure drop with increasing heat flux, as discussed in Section 4.4. In contrast, the performance index increased with increasing base heat flux for the microgap heat sink due to the smaller pressure drop in this heat sink. As noted above, the advantageous performance of the microgap in terms of the performance index is only up to the base heat flux of 250 kW/m^2. After that value, this heat sink is not preferred and cannot be used in cooling applications since a sudden jump in the wall temperature occurs, i.e. critical heat flux is reached. This then makes the microgap a useful alternative choice but for smaller cooling load requirements. At the same time the pressure drop in the heat sink itself is small compared to the overall pressure drop of the thermal management system [20] and hence

the performance index criterion is not necessarily a determining factor in the choice between microgap and multi-channel heat sinks.

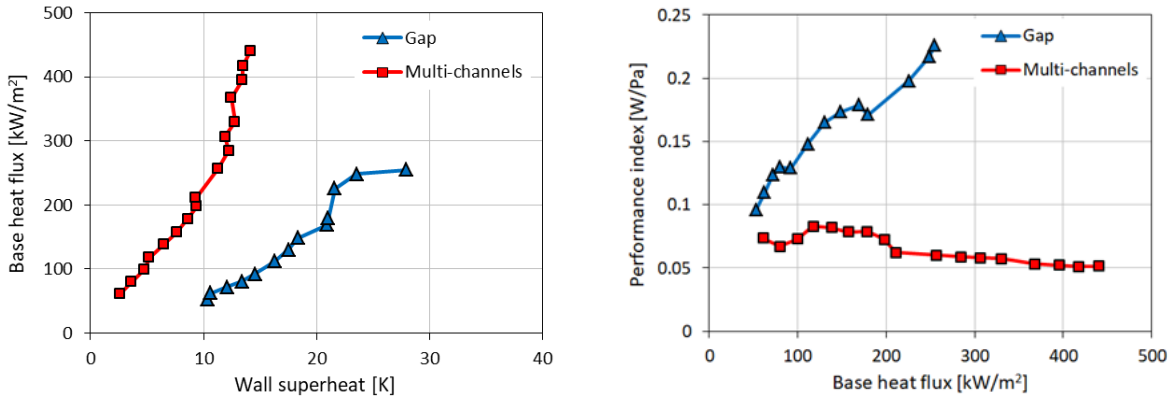

(a) (b)

Fig. 8 Thermal performance of both heat sinks at mass flux of 200 kg/m^2 s: (a) Boiling curve (b) Performance index.

5. CONCLUSIONS

Flow boiling of HFE-7100 in microgap and multi-channel heat sinks was experimentally examined in this study. Flow visualization was also carried out to study the features of the prevailing flow patterns. The mass flux was varied from 100 to 200 kg/m^2 s. The inlet pressure was 1 bar and the degree of sub-cooling was 5 K. The heat flux, based on the heat sink base area of 500 mm^2, was varied from 34 to 440 kW/m^2. The prevailing flow patterns in the multi-channel heat sink were bubbly, slug, churn and annular flow. In the microgap the slug and annular flow, as seen in the multi-channels, were not observed, and the visualised flow can broadly be classified as bubbly, transition and a pattern consisting of vapour layers with liquid straps. The two-phase heat transfer coefficient was higher in the multi-channels compared to that in the microgap. In addition, the critical heat flux condition was reached at a much lower base heat flux values in the microgap, i.e. the CHF was 255 kW/m^2 for the range studied. The maximum base heat flux value in the multi-channel heat sink was more that 440 kW/m^2, i.e. this value was possible without reaching CHF conditions.

The two-phase pressure drop and pressure fluctuations, in the multi-channel heat sink were higher than that reported in the microgap. This resulted in a lower performance index for the former. However, the lower possible CHF for the microgap and the higher substrate temperatures for a given load, place a significant limitation on the range of possible uses as a heat exchanger for high heat flux requirements, i.e. the cooling needs must be below the reported CHF. In addition, the pressure drop in the heat sink is only a fraction of the total pressure drop that needs to be met by the circulating pump in a thermal management system. Therefore, the pressure drop and performance index criterion is not the determining factor in the final choice, i.e. the maximum possible heat transfer rate is the main criterion in the final decision and choice. Modification of the surface of the microgap could possibly result in higher maximum base heat flux and lower surface temperature for a given load, which along with the easy of manufacture, low pressure drop and the better flow stability may improve its viability as an option for electronics cooling.

ACKNOWLEDGMENT

The work was conducted with the support of the Engineering and Physical Sciences Research Council of the UK, under Grant: EP/T033045/1.

NOMENCLATURE

A	Area [m^2]	μ	Viscosity [Pa s]
D_h	Hydraulic diameter [m]	Subscripts	
f	Fanning friction factor [-]	*b*	Base
G	Mass flux [kg/m^2 s]	*ch*	Channel
h	Heat transfer coefficient [W/m^2 K]	*cu*	Copper
$\overline{h}$	Average heat transfer coefficient [W/m^2 K]	*eff*	Effective
k	Thermal conductivity [W/m K]	*exp*	Experiment
L	Length [m]	*f*	Fluid
$\overline{Nu}$	Average Nusselt number [-]	*ht*	Heat transfer
PI	Performance index [W/Pa]	*l*	Liquid
Q	Heat transfer rate [W]	*meas*	Measured
q''	Heat flux [W/m^2]	*sc*	Sudden contraction
Re	Reynolds number [-]	*se*	Sudden expansion
T	Temperature [K]	*sp*	Single-phase
v	Specific volume [m^3/kg]	*th*	Thermocouple
Y	Vertical distance [m]	*tp*	Two-phase
		wi	Internal wall surface
Greek Symbols			
ΔP	Pressure drop [Pa]	*z*	Axial local

REFERENCES

[1] T. G. Karayiannis and M. M. Mahmoud, "Flow boiling in microchannels: Fundamentals and applications," *Appl. Therm. Eng.*, vol. 115, pp. 1372–1397, 2017.

[2] A. H. Al-Zaidi, M. M. Mahmoud and T. G. Karayiannis, "Effect of aspect ratio on flow boiling characteristics in microchannels," *Int. J. Heat Mass Transf.*, vol. 164, p. 120587, 2021.

[3] G. Criscuolo, W. Brix Markussen, K. E. Meyer, B. Palm and M. Ryhl Kærn, "Experimental Characterization of the Heat Transfer in Multi-Microchannel Heat Sinks for Two-Phase Cooling of Power Electronics," *Fluids*, vol. 2, pp. 1–55, 2021.

[4] W. T. Hsu, D. Lee, N. Lee, M. Yun and H. H. Cho, "Enhancement of flow boiling heat transfer using heterogeneous wettability patterned surfaces with varying inter-spacing," *Int. J. Heat Mass Transf.*, vol. 164, 2021.

[5] K. M. Jung, A. Krishnan R, U. Kumar G and H. J. Lee, "Experimental study on two-phase pressure drop and flow boiling heat transfer in a micro pin fin channel heat sink under constant heat flux," *Exp. Heat Transf.*, vol. 34, pp. 162–185, 2021.

[6] N. Tiwari and M. K. Moharana, "Conjugate effect on flow boiling instability in wavy microchannel," *Int. J. Heat Mass Transf.*, vol. 166, p. 120791, 2021.

[7] G. D. Xia, Y. X. Tang, L. X. Zong, D. D. Ma, Y. T. Jia and R. Z. Rong, "Experimental investigation of flow boiling characteristics in microchannels with the sinusoidal wavy sidewall," *Int. Commun. Heat Mass Transf.*, vol. 101, pp. 89–102, 2019.

[8] T. Alam, P. S. Lee, C. R. Yap and L. Jin, "Experimental investigation of local flow boiling heat transfer and pressure drop characteristics in microgap channel," *Int. J. Multiph. Flow*, vol. 42, pp. 164–174, 2012.

[9] R. Ajith Krishnan, K. R. Balasubramanian and S. Suresh, "Experimental investigation of the effect of heat sink orientation on subcooled flow boiling performance in a rectangular microgap channel," *Int. J. Heat Mass Transf.*, vol. 120, pp. 1341–1357, 2018.

[10] A. H. Al-Zaidi, M. M. Mahmoud and T. G. Karayiannis, "Flow boiling of HFE-7100 in microchannels: Experimental study and comparison with correlations," *Int. J. Heat Mass Transf.*, vol. 140, pp. 100–128, 2019.

[11] R. Remsburg, *Thermal design of electronic equipment*. 2001.

[12] H. W. Coleman and W. G. Steele, *Experimentation and uncertainty analysis for engineers*, 3nd ed. New York: Wiley, Chichester, 2009.

[13] R. K. Shah and A. L. London, *Laminar flow forced convection in ducts, Supplement 1 to Advances in Heat Transfer*. Academic Press New York, 1978.

[14] X. F. Peng and G. P. Peterson, "Convective heat transfer and flow friction for water flow in microchannel structures," *Int. J. Heat Mass Transf.*, vol. 39, no. 12, pp. 2599–2608, 1996.

[15] T. Alam, P. S. Lee and C. R. Yap, "Effects of surface roughness on flow boiling in silicon microgap heat sinks," *Int. J. Heat Mass Transf.*, vol. 64, pp. 28–41, 2013.

[16] J. Mathew, P. S. Lee, T. Wu and C. R. Yap, "Experimental study of flow boiling in a hybrid microchannel-microgap heat sink," *Int. J. Heat Mass Transf.*, vol. 135, pp. 1167–1191, 2019.

[17] A. Tamanna and P. S. Lee, "Flow boiling heat transfer and pressure drop characteristics in expanding silicon microgap heat sink," *Int. J. Heat Mass Transf.*, vol. 82, pp. 1–15, 2015.

[18] A. H. Al-Zaidi, M. M. Mahmoud and T. G. Karayiannis, "Flow boiling in copper and aluminium microchannels," *Int. J. Heat Mass Transf.*, vol. 194, p. 123101, 2022.

[19] S. G. Kandlikar, T. Widger, A. Kalani and V. Mejia, "Enhanced flow boiling over open microchannels with uniform and tapered gap manifolds," *J. Heat Transfer*, vol. 135, no. 6, pp. 1–9, 2013.

[20] V.Y.S. Lee, "Flow Boiling of HFE-7200 in Multi-Microchannel Heat Sinks for High-Heat Flux Applications," PhD thesis, Brunel University London, 2020.